Asian Journal of Chemistry; Vol. 26, No. 23 (2014), 7963-7968

ASIAN JOURNAL OF CHEMISTRY

http://dx.doi.org/10.14233/ajchem.2014.16788

Zn and Mn Acetylacetonato Complexes as Precursors for Hexadecylamine-Capped ZnO and MnO Nanoparticles and their Water Solubility

N. FALENI[1] and M.J. MOLOTO[2,*]

[1]Department of Applied Chemistry, University of Johannesburg, P. O. Box 17011, Doornfontein 2028, South Africa
[2]Department of Chemistry, Vaal University of Technology, Private Bag X021, Vanderbijlpark 1900, South Africa

*Corresponding author: Fax: +27 86 7563592; Tel: +27 16 9506689; E-mail: makwenam@vut.ac.za

Received: 29 November 2013; *Accepted*: 3 April 2014; *Published online*: 15 November 2014; AJC-16273

The synthesis of zinc and manganese oxide nanoparticles of uniform sizes and their manipulation from hydrophobic to hydrophilic is described. A single-source precursor route was used by using the metal acetylacetonato complexes. The complexes (Zn and Mn acetylacetonato) were thermolyzed in hexadecylamine to produce ZnO and MnO nanoparticles, which were subsequently made soluble by ligand exchange reaction involving pyridine. Pyridine was replaced by glucose and glucuronic acid in that reaction. The absorption and emission spectra showed the typical features of quantum confinement for all the nanoparticles. The change in the capping groups, from hexadecylamine to glucose and glucuronic acid, resulted in the red shifts in the absorption and emission features. The as-synthesized ZnO and MnO nanoparticles were shown to be stable and soluble in water. The morphology, crystalline form and phase composition of ZnO and MnO nanoparticles were characterized by transmission electron microscopy (TEM) and X-ray diffraction (XRD). The TEM images revealed spherical shaped ZnO and MnO nanoparticles with the average particle size distribution between 2-8 nm. The broadness of the diffraction peaks indicated the presence of small crystallites.

Keywords: Acetylacetonato, Complexes, Hexadecylamine, ZnO, MnO, Nanoparticles.

INTRODUCTION

The synthesis of semiconductor quantum dots has received considerable attention in recent years because of the potential of these materials in many different technological applications and intrinsic interest in the fundamental properties of this form of matter[1-4]. The study of this new class of materials provides an opportunity to investigate properties not generally seen in either bulk or molecular limits. Quantum dots have discrete, large-molecule-like, electronic states that lead to their band-gaps shifting to higher energy with decreasing particle size. The widening of this HOMO-LUMO gap with the decreasing particle size directly affects the photophysical properties of the material. The metal oxide materials are applied in a wide variety of fields, structural ceramics sensors, catalyst, optics and electronics and environmental remediation and magnetic storages[5-11]. Metal oxides nanoparticles are inexpensive, safe and relatively stable and synthesized from very stable chemicals[12]. Several methods have been developed for the synthesis of nanostructured metal oxides, such as, mechano-chemical processing[13], metal alkoxide hydrolysis, alkoxide thermal decomposition, non-hydrolytic sol-gel reaction process[14,15] carbon nanotubes templates[16], non-aqueous synthesis and salt-assisted aerosol decomposition. The preparation of nanostructured metal oxides has a limited usability when using metal organic compounds such as metal alkoxides as sources of the metals. The metal alkoxides are used as precursors; hydrolysis and polycondensation rate can be easily controlled by adjusting the reaction conditions[17-19].

The use of single source molecular precursors of nanoparticles was initially reported by Trindade and O'Brien[20] and these methods have provided efficient routes to high quality crystalline monodispersed nanoparticles of semi-conducting material. This method has been extended to the alkylthiourea metal complexes as precursors to prepare metal sulfide nanoparticles[20,21]. Talapin *et al.*[22] showed that incorporation of alkylamines such as hexadecylamine into the synthesis led to much improved quantum yields. Hexadecylamine ligands with high boiling points are superior agents as growth solvents for high temperature chemical synthesis methods. Recently, high fluorescent colloidal quantum dots with narrow size distribution were synthesized in the presence of hexadecylamine agents[23]. In this work we report the synthesis of zinc(II) acetyl acetonate complexes for use as precursors of ZnO nanoparticles and manganese(II) acetylacetonate complex to produce MnO and we validate the influence of hydrophobic capping group

hexadecylamine on optical properties, size, morphology and solubility of ZnO and MnO nanoparticles in water by capping with hydrophilic groups such as glucose and glucuronic acid. The optical and structural properties of these metal oxides nanoparticles were thoroughly studied and reported.

EXPERIMENTAL

Toluene, acetylacetone, urea and zinc chloride used in the synthesis were analytical grade reagents. Tri-*n*-octylphosphine (TOP), hexadecylamine (HDA), pyridine, ethyl acetate, chloroform and manganese (II) acetylacetonate [$Mn(C_5H_8O_2)_2$] were all purchased from Sigma Aldrich and used as supplied without further purified.

UV-visible and FT-IR spectroscopic measurements: The absorption spectra of ZnO and MnO nanoparticles were taken using a Analytikjena SPECORD 50 UV-visible spectrophotometer and the emission spectra were recorded on a LS 45 Perkin-Elmer fluorimeter with a xenon lamp at room temperature using methanol as a solvent. Surface interaction of glucose on the nanoparticles of all the samples was characterized using FT-IR Perkin Elmer 100 spectrometer. Measurements were performed by manually placing the solid sample on a diamond tip and pressed for analyses.

Electron microscopy: The transmission electron microscopy (TEM) and high resolution TEM images were obtained using a JEM -2100 JEOL electron microscope. The samples were prepared by placing a drop of a dilute solution of sample in methanol on a copper grid.

X-Ray diffraction: X-Ray diffraction (XRD) patterns on powdered samples were measured on Phillips X'Pert materials research diffractometer using secondary graphite monochromated CuK_α radiation (λ = 1.54060 Å) at 40 kV/50 mA. Measurements were taken using a glancing angle of incidence detector at an angle of 2º, for 2θ values over 20º-70º in steps of 0.05º with a scan speed of 0.05º 2θ s^{-1}.

Synthesis of hydrophobic metal oxide nanoparticles using the single source precursor route: Hexadecylamine (HDA) (3 g) was added into a three-necked flask and heated to 160 ºC under nitrogen flow. Then zinc acetylacetonato complex (1 g, 3.79 mmol) was dispersed TOP (10 mL) and then the solution was injected into hot hexadecylamine under stirring and turned yellow. The heating was continued for about 1 h and then the reaction mixture was cooled to 70 ºC. The same procedure was followed for synthesis of MnO nanoparticles and the solution turned brown.

Synthesis of $Zn(C_5H_8O_2)_2$: Zinc chloride (1 g, 8 mmol) was dissolved in distilled water (10 mL) and then urea solution (2.3 g, 38 mmol) which was dissolved in acetylacetone (5.0 mL) was added to the zinc solution. The mixture was stirred and refluxed for about 3 h, then after reaction mixture was cool to room temperature. The resulting product was filtered and washed several times with methanol (30 mL each time) and left to dry overnight at room temperature. The complex was further purified by refluxing in methanol (50 mL) to give white powder. $Zn(acac)_2$ complex: yield; 3.8 g (60.5 %). m.p. 136-138 °C. Anal. calc.: for $C_{10}H_{16}O_4Zn$; C, 45.3; H, 6.04; Found: C, 45.4; H 6.7. FT-IR (cm^{-1}): 2908(m), 1683(m), 1236(m), 1087(s), 891(s). The $Mn(acac)_2$ complexes was purchased and used.

Synthesis of hydrophilic metal oxide nanoparticles

Ligand exchange with pyridine: Hexadecylamine-capped ZnO, (1 g) was added to pyridine (5 mL) and the reaction mixture was heated to 40 °C while vigorously stirring for 1 h. After cooling to room temperature, hexane (10 mL) was added to the mixture to precipitate the nanoparticles and once the precipitate settled down, the supernatant was then decanted. The water-soluble capping agent solutions, glucose (3 g, 16.7 mmol) and glucuronic acid (3 g, 15.5 mmol) were prepared in methanol (30 mL in each case) and added to the two reaction mixtures. The mixtures were then heated to 40 °C for about 1 h at and then left to cool at room temperature. Chloroform (5 mL) and ethyl acetate (5 mL) were added to the two reaction mixtures to precipitate the nanoparticles in subsequent, then followed by the addition of diethyl ether (10 mL) in each mixture to remove an excess pyridine from the reaction mixtures. The same procedure was conducted for hexadecylamine-capped MnO nanoparticles. The resulting products were centrifuged and the solid products were isolated and dried for analysis.

Solubility test: A solubility tests were performed in order to investigate the surface properties of the nanoparticles. An equal amount of nanoparticles synthesized using the respective capping agents were dissolved in an equal amount of water. The solubility test procedure was based on an attempt to dissolve water-soluble metal oxide nanoparticles in distilled water with an increasingly rigorous mechanical technique such as an ultrasonicator. The solvent (distilled water) was much favored for dissolving the synthesized water-soluble metal oxide nanoparticles as a clear solution was observed and no signs of cloudiness.

RESULTS AND DISCUSSION

Metal acetylacetonato precursors are not as common as metal alkoxides or metal halides for the synthesis of metal oxide nanoparticles, regardless of their widely available commercially and are inexpensive[24]. However, in this study we used zinc acetylacetonato and manganese acetylacetonato were used as general precursors for the synthesis of ZnO and MnO nanoparticles, respectively. All the intermediates and final products were obtained in good yields and their elemental analysis was in agreement with the calculated one.

One of the impressive features of those semiconductor nanoparticles is their ability to emit light. The optical spectra of hexadecylamine capped ZnO and MnO nanoparticles are depicted in Fig. 1 (i) and (ii), which shows multiple peaks arising from different transitions. Their absorption band-edge [Fig.1 (i)] at 312 nm is blue-shifted in relation to the bulk band edge of 375 nm, a large blue-shift associated with the strong quantum confinement effects. In Fig. 1 (ii) (a-b) is characterized by two peaks with the first peak the excitonic (261 nm) and the absorption band at 325 nm respectively and blue shifted in relation to the bulk 2.2 eV (563 nm). As the nanocrystals becomes very small compared to the Bohr exciton radius and approaches the size of the atom, the energy levels of zinc oxide nanoparticles becomes quantized[25]. However, the extent of the blue-shift could be contributed to the presence of defects, which is the gradual removal of the initial trap and

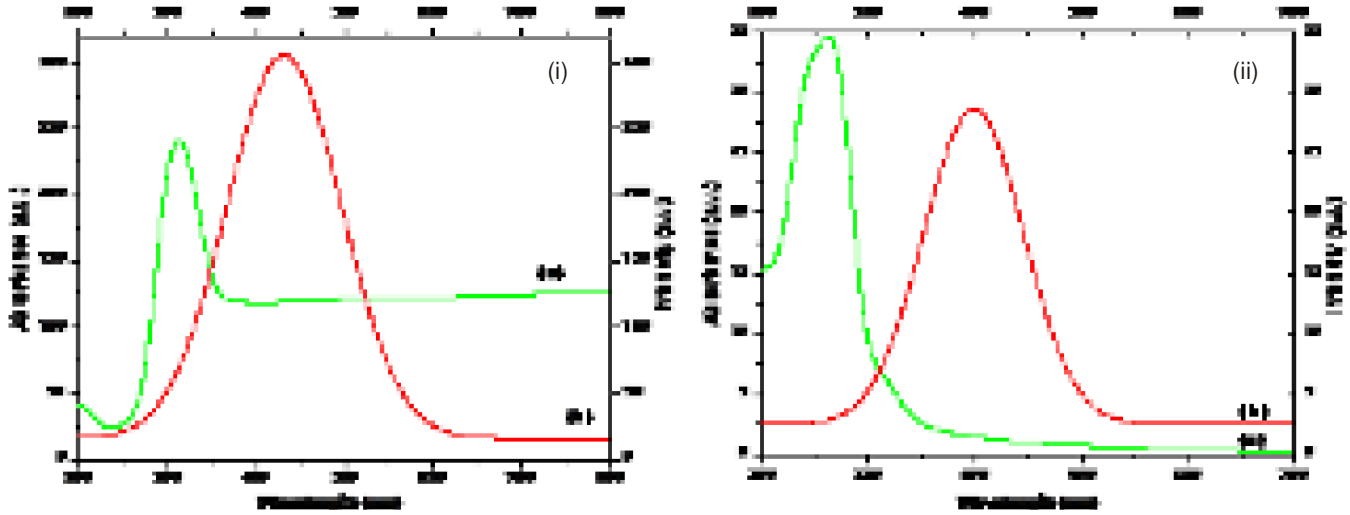

Fig. 1. Absorption (a) and photoluminescence (b) spectra of hexadecylamine-capped (i) ZnO and (ii) hexadecylamine-capped MnO nanoparticles

surface states during the crystallization process of nanoparticles[26]. The photoluminescence spectrum is red-shifted from the absorption band-edge and the maximum emission peak is located at 433 nm ZnO (i) and 420 nm MnO (ii) (b). The red-shifted emission band of ZnO and MnO nanoparticles arises to either shallow traps or dark excitons arising from fine-structure splitting[27-29].

Optical characterization does not definitively define the physical attributes of the nanoparticles and therefore structural characterization was performed on the synthesized products. X-ray diffraction can establish the composition, phase and crystallinity of the particles. The XRD patterns in Fig. 2 (i) and 2 (ii) shows the hexadecylamine capped zinc oxide and manganese oxide nanoparticles. As can be seen from Fig. 2 (i) that the peaks were indexed to a hexagonal ZnO phase (JCPDS, 31-0228) and tetragonal hausmannite, Mn_3O_4 (JCPDS, 80-0382) [Fig. 2(ii)] for MnO, with the average particle size of 20 and 24 nm calculated using the Scherrer equation[30]. The three predominant peaks between 22º and 28º can be indexed to 100, 002 and 101 planes for ZnO are further confirming the hexagonal phase. Whereas for manganese oxide where indexed at 19.5º = 112, 22º = 103 and 25º = 211, respectively. The broadness of the diffraction peaks is an indication of the presence of small crystallites. The presence of hexadecylamine detected is marked with (†). These observations were also verified the during synthesis of hexadecylamine capped CdS nanoparticles[31].

The structural properties of the hexadecylamine capped ZnO nanoparticles were further characterized by TEM in order to establish the size, morphology and the crystallinity of the particles. The TEM in Fig. 3 (i) shows respectively confirm the size and the spherical morphology of the nanoparticles. The micrographs showed nearly monodispersed spherical particles with diameters in the range of approximately 8-10 nm.

Fourier transform infrared (FTIR) spectroscopy allows the detection of complex formations on the surface of nanocrystals and to point out the implication of the capping groups with ZnO and MnO nanoparticles and analyzing the significant changes in the shape and position of the transmission bands. It can be seen that the C-N vibration peak (1465 cm^{-1}) and C-H peak (1652 cm^{-1}) of hexadecylamine are observed, whereas the N-H asymmetric stretch peak (3400-3200 cm^{-1}) is slightly weaker and broader due to the amine ligands bound to the nanoparticles surfaces (Fig. 4). This observation demonstrates

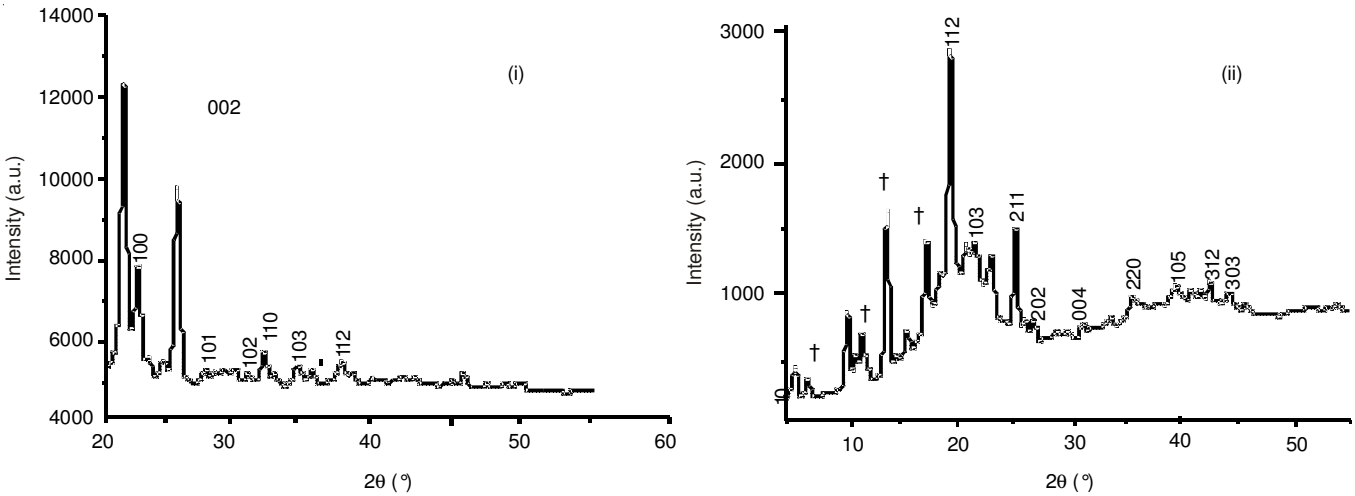

Fig. 2. X-ray diffraction pattern of (i) hexadecylamine capped ZnO and (ii) hexadecylamine capped MnO nanoparticles (†denotes excess hexadecylamine)

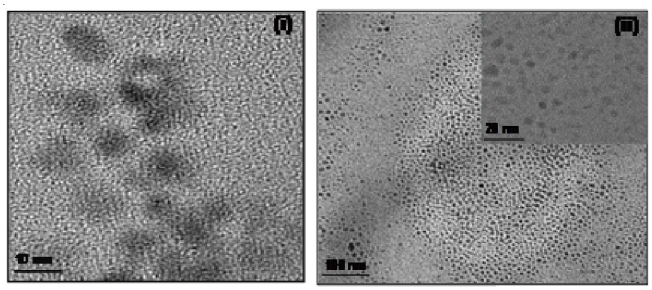

Fig. 3. TEM image of (i) hexadecylamine-capped ZnO and (ii) hexadecylamine-capped MnO nanoparticles

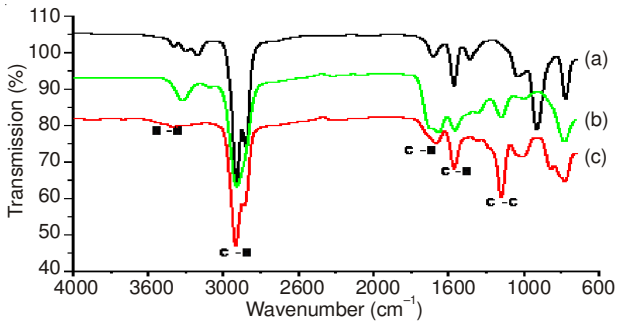

Fig. 4. FT-IR spectra of hexadecylamine free (a), hexadecylamine-capped for both (b) MnO and (c) ZnO nanoparticles

that the nanospheres were stabilized by hexadecylamine. Similar observations have been observed in hexadecylamine-capped semiconductorsl[32].

Ligand exchange experiments for the synthesis of hydrophilic metal oxides (Zn, Mn) nanoparticles: This method involves the displacement of hydrophobic ligands with hydrophobic moieties that coordinate with surface atoms in the outermost layer. Ligand exchange methods do not change the whole particle size much and are suitable for large-scale production. In the first described ligand exchange experiments[33], the ligand used was mercapto-acetic acid, which possesses a -SH binding group and a carboxylic group, which provides water solubility through the repulsive electrostatic interactions of the charged COO^- groups[34]. Other methods beside ligand exchange were also employed to convert hydrophobic to hydrophilic nanoparticles. This is recommended according to the monodispersity of the nanoparticulates, high fluorescence, narrow emission, broad UV excitation and high photostability

The optical absorption (UV) and photoluminescence (PL) spectra in Fig. 5(i) and (ii) shows curves of glucose and glucuronic acid capped ZnO and MnO ((iii) and (iv) nanoparticles. The absorption spectrum (in Fig. 5 (i)) for glucose capped

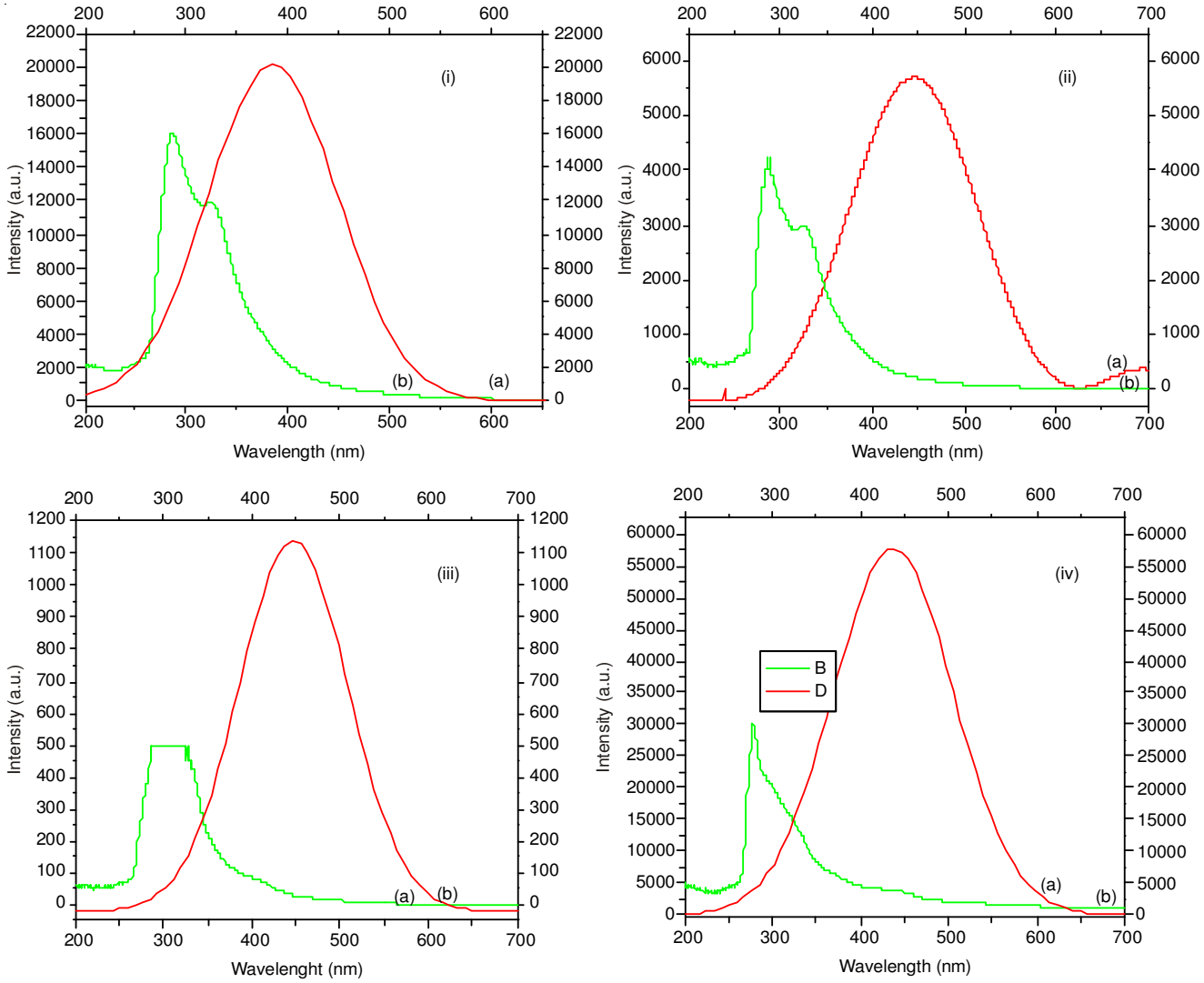

Fig. 5. Absorption (b) and emission (a) spectra of: ZnO (i) 0.5 g glucose and (ii) 0.5 g glucuronic acid capped and MnO (iii) and (iv) nanoparticles

ZnO nanoparticles shows a sharp excitonic feature at 260 nm with the absorption band edge at 324 nm. The blue shift is due to the particles nanosize regime exhibiting quantum confinement effect.

A stronger confinement leads to a larger separation of the energetic levels. As a result higher energy is required to promote an electron from the valence band to the conduction band. However, the wavelength maximum emissions are red shifted from the absorption peak at 445 nm and this is a typical feature of well passivated nanoparticles[29].

The absorption band edges of the glucose and glucuronic acid-capped ZnO nanoparticles [Fig 5 (i) and (ii)] appeared at 324 and 322 nm, respectively, with blue shifts of about 45-47 nm. Their corresponding emission maxima were observed at 445 nm for both glucose and glucuronic acid capped ZnO nanoparticles. The broadness of the PL peak for glucuronic acid capped nanoparticles are indicative of wide size distribution of particles.

The absorption spectra of water-soluble manganese oxide nanoparticles are depicted [Fig. 5 (iii) and (iv)] for glucose and glucuronic acid capped MnO nanoparticles. The result the excitonic peaks center was recorded at 280 nm and it was blue shifted from bulk MnO band edge (563 nm). This is due to the quantization of the energy levels in the valence and conduction bands of the nano-semiconductor causing an increment of the band-gap energy[33]. The photoluminescence is red-shifted from the absorption band-edge (λ_{max} = 450 nm) as a result of irradiative energy losses. The spectrum is normally distributed portraying a monodispersed sample as well as good surface passivation of the nanoparticles by the capping.

The X-ray diffractograms in Fig. 6 (i) (a) and (b) shows particles of glucose and glucuronic acid capped ZnO nanoparticles with peaks between 22º and 28º indexed to hexagonal wurzite phase, with predominant peaks indexed to 100, 002 and 101 planes. XRD patterns in [Fig. 6 (ii) (a) and (b)] for glucose and glucuronic acid capped manganese oxides nanoparticles were indexed to face-centered cubic MnO phase (manganosite) and tetragonal Mn_3O_4 (hausmannite). However, careful inspection of the asymmetric necks of 111 and 220 peaks at 2θ = 34.91º and 58.21º of manganosite indicates the presence of another phase hausmannite The diffractograms showed some crystallinity with the evidence of peak broadening, suggesting the formation of small crystallites. The produced nanoparticles are small and they reduce the surface area by agglomeration.

The structural properties of the water-soluble capped ZnO nanoparticles were characterized by TEM. The TEM micrographs [Fig. 7 (i) and (ii)] show nearly monodispersed spherical particles with diameters in the range of 6-8 nm for glucose and glucuronic acid capped ZnO nanoparticles. This respectively confirms the size and spherical morphology of the nanoparticles. The corresponding glucose and glucuronic acid capped manganese oxide nanoparticles in Fig. 7 (iii) and (iv) shows spherical nanoparticles with approximate diameters between 2-5 nm.

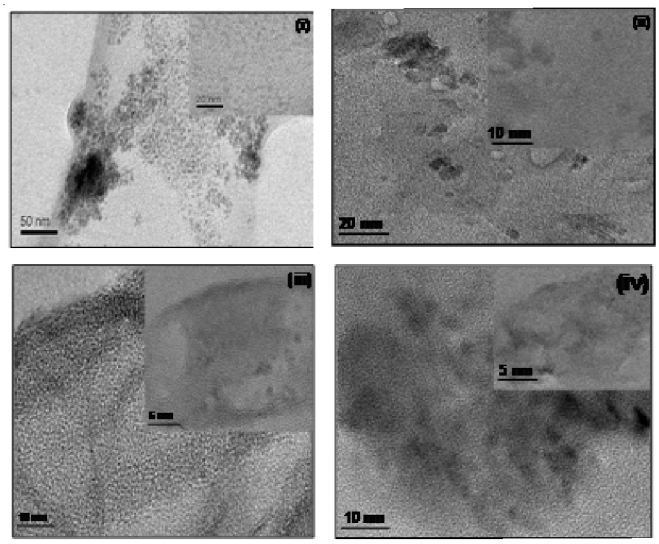

Fig. 7. TEM micrographs of ZnO (i) glucose and (ii) glucuronic acid capped MnO (iii) and (iv) synthesized from hexadecylamine-capped ZnO and MnO nanoparticles

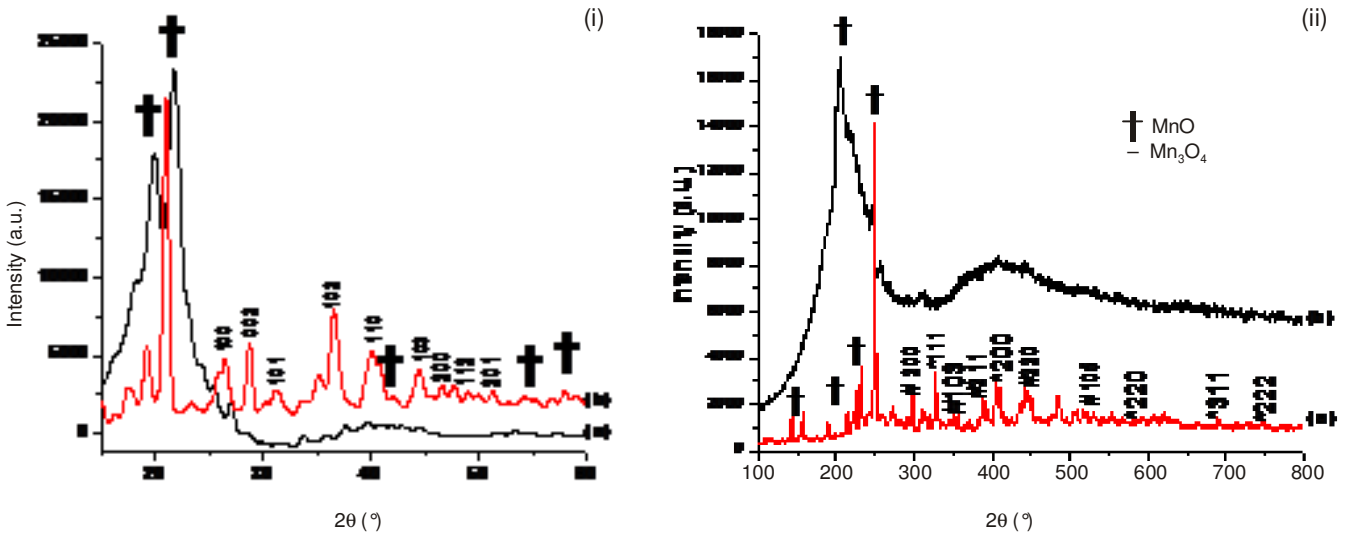

Fig. 6. X-ray diffraction patterns of (a) glucose and (b) glucuronic acid capped (i) ZnO and (ii) MnO synthesized from hexadecylamine-capped ZnO and MnO nanoparticles

A solubility tests were performed in order to investigate the surface properties of the nanoparticles. The concentration was then measured to establish the solubility of the particles (Fig. 8). The solubility test revealed that the glucose and glucuronic acid capped ZnO nanoparticles were 80 and 40 % soluble in water. This suggests that the particles were effectively capped. Whereas, 60 and 30 % for glucose and glucuronic acid capped MnO nanoparticles were soluble in water. The solubility of MnO nanoparticles is affected by the contribution of manganese oxide into water hardness. This is might be attributed to the agglomeration was observed in Fig. 8 for glucose and glucuronic acid capped MnO nanoparticles.

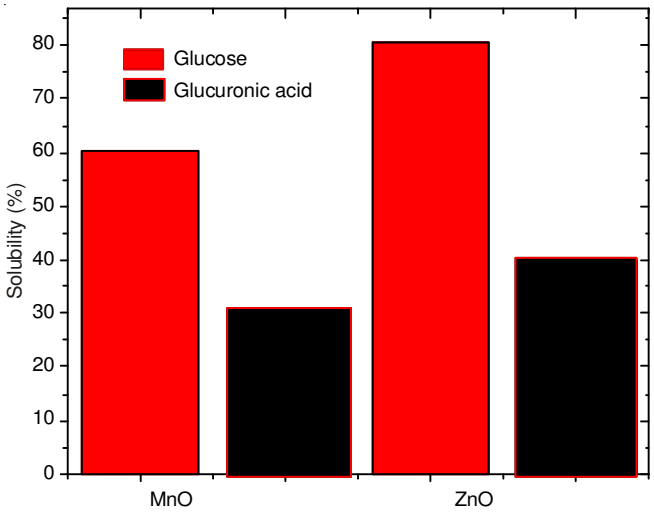

Fig. 8. Water solubility graph of glucose and glucuronic acid capped ZnO and MnO nanoparticles, (synthesized from single source precursor route)

Conclusion

Metal acetylacetonato complexes were used successfully as precursors of metal oxide nanoparticles with sugar molecules varied from hexadecylamine to glucose and glucuronic acid. Both ZnO and MnO nanoparticles in both capping agents gave blue shifted band edges and red shifted emission maxima. Ligand exchange resulted in slight changes in size of nanoparticles range and also XRD reveals the presence of hexadecylamine which was not removed completely on the surface of nanoparticles. TEM images revealed particles with high level of monodispersity and average particle size distribution 2 to 8 nm for both ZnO and MnO in both capping molecules. The solubility test revealed that glucose was a more effective ligand for rendering the nanoparticles water soluble.

ACKNOWLEDGEMENTS

This work was supported by the National Research Foundation of South Africa, University of Johannesburg and Vaal University of Technology.

REFERENCES

1. A. Eychmüller, *J. Phys. Chem. B*, **104**, 6514 (2000).
2. A.P. Alivisatos, *Science*, **289**, 736 (2000).
3. R. Vacassy, C. Guizard, J. Palmeri and L. Cot, *Nanostruct. Mater.*, **10**, 77 (1998).
4. C.R. Xia, H.Q. Cao, H. Wang, P.H. Yang, G.Y. Meng and D.K. Peng, *J. Membr. Sci.*, **162**, 181 (1999).
5. H. Kurosawa, Y.T. Yan, N. Miura and N. Yamazoe, *Solid State Ion.*, **79**, 338 (1995).
6. J. Riegel, H. Neumann and H.-M. Wiedenmann, *Solid State Ion.*, **152**, 783 (2002).
7. N. Miura, M. Nakatou and S. Zhuiykov, *Sens. Actuators B*, **93**, 221 (2003).
8. W. Li, S.Y. Yu and E. Iglesia, *J. Mol. Catal. Chem.*, **203**, 175 (2001).
9. A. Knell, P. Barnickel, A. Baiker and A. Wokaun, *J. Catal.*, **137**, 306 (1992).
10. J. Gottmann and E.W. Kreutz, *Surf. Coat. Technol.*, **116-119**, 1189 (1999).
11. W. Stichert and F. Schüth, *Chem. Mater.*, **10**, 2020 (1998).
12. N.R. Jana, Y. Chen and X. Peng, *Chem. Mater.*, **16**, 3931 (2004).
13. P.G. McCormick, T. Tsuzuki, J.S. Robinson and J. Ding, *Adv. Mater.*, **13**, 1008 (2001).
14. H. Kominami, M. Kohno, Y. Takada, M. Inoue, T. Inui and Y. Kera, *Ind. Eng. Chem. Res.*, **38**, 3925 (1999).
15. K. Okuyama, Y. Kousaka, N. Tohge, S. Yamamoto, J.J. Wu, R.C. Flagan and J.H. Seinfeld, *AIChE J.*, **32**, 2010 (1986).
16. J. Joo, T. Yu, Y.W. Kim, H.M. Park, F. Wu, J.Z. Zhang and T. Hyeon, *J. Am. Chem. Soc.*, **125**, 6553 (2003).
17. J. Tang, J. Fabbri, R.D. Robinson, Y. Zhu, I.P. Herman, M.L. Steigerwald and L.E. Brus, *Chem. Mater.*, **16**, 1336 (2004).
18. C.N.R. Rao, B.C. Satishkumar and A. Govindaraj, *Chem. Commun.*, 1581 (1997).
19. G. Oskam and F.J.P. Poot, *J. Sol-Gel Technol.*, **37**, 157 (2006).
20. T. Trindade, P. O'Brien and X. Zhang, *Chem. Mater.*, **9**, 523 (1997).
21. M.J. Moloto, N. Revaprasadu, P. O'Brien and M.A. Malik, *J. Mater. Sci. Mater. Electron.*, **15**, 313 (2004).
22. D.V. Talapin, A.L. Rogach, A. Kornowski, M. Haase and H. Weller, *Nano Lett.*, **1**, 207 (2001).
23. M. Mlambo, M.J. Moloto, N. Moloto and P.S. Mdluli, *Mater. Res. Bull.*, **48**, 2196 (2013).
24. T. Tsuchiya, A. Watanabe, Y. Imai, H. Niino, I. Yamaguchi, T. Manabe, T. Kumagai and S. Mizuta, *Jpn. J. Appl. Phys.*, **38**, L1112 (1999).
25. H. Haug and S.W. Koch, Quantum Theory of the Optical and Electronic Properties of Semiconductors, World Scientific Publishing Company, Incorporated, edn. 3 (1994).
26. K.A. Willis, A.W. Ammerman and M. Lauren, *Chem. Commun.*, **47**, 9507 (2011).
27. L. Guo, S.H. Yang, C.L. Yang, P. Yu, J.N. Wang, W.K. Ge and G.K.L. Wong, *Appl. Phys. Lett.*, **76**, 2901 (2000).
28. C.A. Smith, H.W. Lee, V.J. Leppert and S.H. Risbud, *Appl. Phys. Lett.*, **75**, 1688 (1999).
29. M. Kuno, J.K. Lee, B.O. Dabbousi, F.V. Mikulec and M.G. Bawendi, *J. Chem. Phys.*, **106**, 9869 (1997).
30. C. Montgomery and D. Montgomery, *Phys. Rev.*, **56**, 10 (1939).
31. P.M. Shumbula, M.J. Moloto, T.R. Tshikhudo and M. Fernandes, *S. Afr. J. Sci.*, **106**, 7 (2010).
32. R.W. Meulenberg, S. Bryan, C.S. Yun and G.F. Strouse, *J. Phys. Chem. B*, **106**, 7774 (2002).
33. W.C.W. Chan and S. Nie, *Science*, **281**, 2016 (1998).
34. A.M. Derfus, W.C.W. Chan and S.N. Bhatia, *Adv. Mater.*, **16**, 961 (2004).